Control and measurement of ultrashort pulse shapes (in amplitude and phase) with femtosecond accuracy

Jean-Claude M. Diels, Joel J. Fontaine, Ian C. McMichael, and Francesco Simoni

The performances of a tunable femtosecond dye laser are analyzed using accurate correlation techniques. The source is a passively mode-locked dye laser, of which both the frequency and frequency modulation are controlled by one or two intracavity prisms. Interferometric second-order autocorrelations, with a peak-to-background ratio of 8 to 1, are used simultaneously with the conventional intensity autocorrelation and the pulse spectrum to determine the pulse shape. The main advantages of the interferometric autocorrelations are that they provide phase information otherwise not available, and they are more sensitive to the pulse shape than the intensity autocorrelation. The phase sensitivity is demonstrated in an analysis of the Gaussian pulses with a linear frequency modulation. Analytical expressions for the envelopes of the interferometric autocorrelations of typical pulse shapes are provided for quick pulse shape identification. A numerical method is used to analyze the more complex pulse shapes and chirps that can be produced by the laser. A series of examples demonstrates the control of this laser over various pulse shapes and frequency modulations. Pulse broadening or compression by propagation through glass is calculated for the pulse shapes determined from the fittings. Comparisons of autocorrelations and cross correlations calculated for the dispersed pulses, with the actual measurements, demonstrate the accuracy of the fitting procedure. The method of pulse shape determination demonstrated here requires a train of identical pulses. Indeed, it is shown that, for example, a train of unchirped pulses randomly distributed in frequency can have the same interferometric autocorrelation than a single chirped pulse. In the case of the present source, a comparison of the pulse spectrum, with that of the second harmonic, gives an additional proof that pulse-to-pulse fluctuations are negligible.

I. Introduction

Recent progress in mode-locked dye lasers led to the development of stable sources generating a continuous train of pulses of <100-fsec duration.[1–4] Since electronic detection techniques are still limited at around 1 psec for the fastest streak cameras, there is a need for methods to resolve the phase and amplitude modulation of the ultrashort pulses. In principle, successive optical correlations of increasing order (2,3 . . . n) would provide the answer. One chooses generally to remain at order 2 with second harmonic detection, mainly because the low energy/pulse (in the case of unamplified pulse trains from the laser) makes it impractical to use higher-order processes. This problem is compounded by the bandwidth requirement (the bandwidth of the nonlinear process has to exceed that of the short pulse) which prevents the use of resonantly enhanced nonlinearities. Unfortunately second-order autocorrelations, being symmetrical functions, cannot provide unequivocal information on the pulse shape and in particular its asymmetry. Moreover, the intensity autocorrelations that are generally used are very insensitive to the particular pulse shape.

When performed with interferometric accuracy, second-order autocorrelations provide a much more contrasted pattern[5]: the envelope of the constructive interferences has a peak-to-background ratio of 8 to 1 (against 3 to 1 for conventional intensity autocorrelations). Because the intensity of the second harmonic sum field is measured, the fourth power of the electric field amplitude is involved. The interferometric autocorrelations are therefore very sensitive to the exact pulse shape. Unlike intensity autocorrelations where all phase information is averaged out, various types of chirp produce distinctive patterns in the interferometric autocorrelations. A simultaneous measurement of the

When this work was done all authors were with North Texas State University, Department of Physics, Center for Applied Quantum Electronics, Denton, Texas 76203; J. J. Fontaine is now with Ecole Nationale Superieure des Arts et Industries de Strasbourg, 67000 Strasbourg, France, I. C. McMichael is now with Rockwell International Corporation, Science Center, Thousand Oaks, California 91360, and F. Simoni is now with Universita della Calabria, Dipartimento di Fisica, 87030 Cosenza, Italy.

Received 17 December 1984.
0003-6935/85/091270-13$02.00/0.

spectrum, second-order intensity autocorrelation, and second-order interferometric autocorrelation[6] provides enough information to determine the pulse shape in amplitude and phase. We have demonstrated this method on a femtosecond laser with controllable chirp and frequency, described in Sec. II. The standard intensity autocorrelation measurement and its limitations are discussed in Sec. III. The general properties of the interferometric autocorrelations are reviewed in Sec. IV. Different classes of pulse have typical shapes for the upper and lower envelopes of the interferometric autocorrelation. A particularly simple and important case is that of linearly chirped Gaussian pulses, which is treated analytically in Sec. V. Quick identification of Gaussian, sech, and simple asymmetric shapes is also possible through identification of the measurements with corresponding analytical expressions given in Sec. VI. A more tedious trial and error numerical approach is required with pulses of arbitrary shape and modulation, as illustrated for real pulses with and without phase modulation, generated by the laser (Sec. VII). Pulse broadening and phase modulation through dispersion in glass offers a simple check to the diagnostic method (Sec. VIII). Downchirped pulses are compressed through propagation in glass. The compressed pulse can be used as a probe to verify—by cross correlation—the shape of the downchirped pulse (Sec. IX). Since, as noted previously, all these techniques use second harmonic detection, it is important to verify that no spectral filtering occurs through the nonlinear process (Sec. X).

II. Laser Source

Several techniques are presently available to generate trains of pulses of a duration of <100 fsec. The output of synchronously pumped dye lasers can be phase modulated in single-mode fibers and thereafter compressed in a dispersive delay line.[7] These pulse durations can also be obtained directly from passively mode-locked ring lasers.[1–4] The two counterpropagating pulses meeting in the saturable absorber result in an enhanced saturation (compared with the saturation by a single pulse as in the linear laser cavity). Theoretical studies have shown that the shortest achievable pulse duration in these lasers is related to the absorber jet thickness. Indeed, for pulses longer than the jet thickness, a larger compression factor/pass is predicted for the colliding pulses, compared to the single traveling pulse situation.[8,9] However, for pulses shorter than the jet thickness, the population grating induced by the colliding pulses results in a mutual coupling of the front of each pulse into the tail of the other, counteracting the pulse compression mechanism.[10] The saturation of the dye diethyloxadicarbocyanine iodide (DODCI) is rather complex, because of the simultaneous presence of ground state DODCI, with peak extinction coefficient at 590 nm, and its optical isomer, for which the absorption peaks at 615 nm, near the center of the laser tunability range. We estimate ~10% of an optical isomer to be contributing to the saturable absorption, which implies a combination of a resonant and a nonresonant contribution. The off-resonant saturation causes self-phase modulation of the pulses. The single-pass downchirp induced by off-resonance interactions with the absorber has been calculated to be $\Delta\omega/\tau \cong 1/(2\tau^2)$ for τ = 50-fsec pulses.[11,12] In most ring cavities, such a downchirp can be compensated by the dispersion of one of the mirror coatings used near a transmission edge[13] (since these are the only losses defining the wavelength of operation in these lasers). Most of the measurements described in this paper were performed with the laser cavity sketched in Fig. 1. Thanks to the use of a standard tuning prism, broadband coatings (as opposed to edge reflectors or narrowband mirrors) can be used near the center of their reflection band for all cavity mirrors. There are now four elements contributing to phase modulation and dispersion in the cavity: the absorber jet, the glass dispersion, mirror coating dispersion, and cavity dispersion. The amount of intracavity glass can be adjusted to compensate for (negative) dispersion and self-phase modulation. The very strong dependence of intracavity compensating glass on the intensity in the absorber (as modified by moving the jet out of focus) clearly demonstrates that self-phase modulation is the dominant downchirping mechanism. Calculations[11,12,14] indicate that the downchirp is equivalent in magnitude to the upchirp produced by a glass path of 2 mm of quartz. The dispersion of the broadband coatings has been calculated[12,13,15] to be equivalent to only 0.15 mm of quartz at most. These calculations were confirmed experimentally by measuring the change in quartz thickness required for intracavity chirp compensation for nearly identical mirrors differing only in their center wavelength. The fourth dispersive effect—cavity dispersion—was pointed out recently by Gordon and Fork.[16] Because of the cavity geometry, one expects a nonzero $d^2L/d\lambda^2$, where L is the cavity perimeter. Because it is intrinsic to the whole cavity, this effect is difficult to measure independently from self-phase modulation in the absorber jet. Measurements of the dependence of chirp compensation on the position of the absorber jet[12,17] indicate that this effect

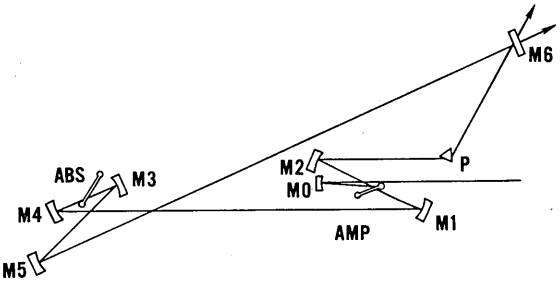

Fig. 1. Sketch of the laser cavity. Mirrors of 5-cm radius of curvature were used around the amplifier dye jet ($M0$, $M1$, and $M2$), and 3-cm curvature around the saturable absorber jet ($M3$ and $M4$). The mirror $M5$ has a radius of curvature of 1 m. Transmission factors ranging from 2% to 10% were used for the output coupler $M6$. To adjust the amount of intracavity glass, the prism P is mounted on a translation stage oriented along the bisector of the angle made by the beams leaving the prism.

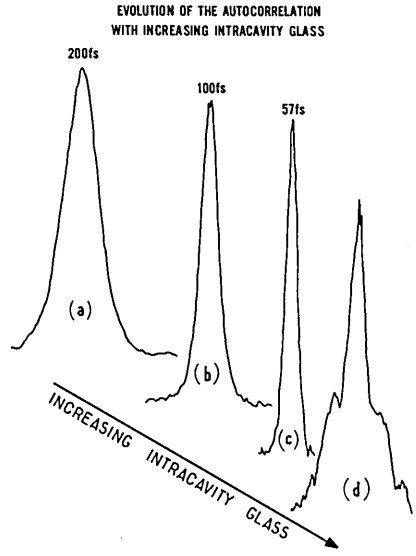

Fig. 2. Successive intensity autocorrelations taken for increasing amounts of intracavity glass.

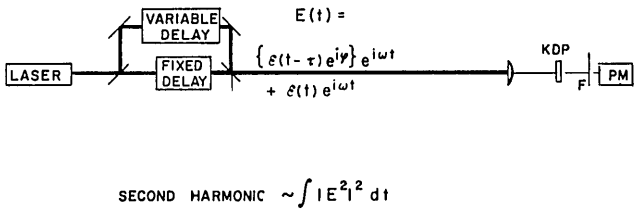

Fig. 3. Sketch of a second-order autocorrelation measurement. Optical delay lines are used to split the original laser pulse in a sequence of two pulses of relative phase ϕ and delay τ. The second harmonic of that pulse sequence, generated in a KDP crystal, is detected through the color filers F (to eliminate the fundamental radiation) by the photomultiplier tube PM.

is smaller than self-phase modulation.

The cavity sketched in Fig. 1 is particularly well suited to demonstrating the series of diagnostics presented below, because the pulse duration and phase modulation can be continually adjusted and because of the accurate pulse-to-pulse reproducibility (as demonstrated by the pulse dispersion–pulse compression measurements of Sec. VIII and the cross correlations of Secs. IX and X).

The curvature of the focusing mirrors at the absorber (DODCI and DQOCI) is 3 cm, against 5 cm for the mirrors at the gain jet. The requirement of spatial chromaticity imposes an uneven (minimum three) number of focal spots in this cavity (to ensure an inverted image of the prism after each round trip). In one direction, the effect of the angular dispersion of the prism is reduced by the small distance between the gain jet and the prism. In the other direction, the various spectral components are recollimated in the cavity by a 1-m curvature mirror ($M3$). The prism is used at minimum deviation angle and mounted on a translation stage to vary the amount of intracavity glass without perturbing the alignment. The effect of adjusting the thickness of intracavity glass is illustrated by the succession of intensity autocorrelations displayed in Fig. 2. The pulse duration is seen to decrease to a minimum with increasing intracavity glass. Further increase of intracavity glass beyond the optimum value generally leads to a breakup of the intensity autocorrelation [(d) in Fig. 2] indicating satellite pulses and unstable operation. In some instances it has been possible to observe well-defined mode-locked pulses of increasing duration (with increasing glass thickness beyond the optimum value). The disadvantage of this cavity is the complexity of alignment due to the large number of optical elements. We believe that future application will involve a linear structure terminated by an antiresonant ring.[13,18] This laser combines the advantages of the linear laser (ease of alignment, all the power in one output beam, adjustable cavity length) with some of those of the ring laser (colliding pulse mode locking).

III. Characterization of Pulses by Intensity Autocorrelations

The basic elements of a second-order autocorrelation setup are sketched in Fig. 3. The pulse train is split into two beams which are recombined after having passed through a fixed and adjustable optical delay. The average power of the second harmonic of the recombined beam (generated in a KDP crystal) is recorded as a function of the variable delay. The function that is recorded is proportional to $\int |(E_t)^2|^2 dt$, where $E_t = E(t) + E(t - \tau)$ is the electrical field of the light entering the frequency doubler KDP crystal. If interference fringes in the recombined beam are averaged out, it can be shown[5,19–21] that the recorded signal is proportional to

$$Ic_1 = 1 + 2\{I(t)I(t - \tau)dt\}/\{\int I^2 dt\}, \quad (1)$$

where I is the intensity of the light pulse. The function Ic_1 has a peak-to-background ratio of 3 to 1. In some experimental arrangements, only the function

$$I_c = \int I(t)I(t - \tau)dt/\int I^2 dt \quad (2)$$

is measured.[22] I_c is called the background-free autocorrelation. The function I_c (or Ic_1) does not carry any phase information and therefore cannot be used to distinguish coherent from incoherent pulses. Yet the use of the expression "coherent spike", associated with the intensity autocorrelation, has sometimes created some confusion by making it appear as if a pulse free of coherent spike (in its autocorrelation) is a coherent pulse. We summarize therefore some of the properties and information contained in the intensity autocorrelation to clarify the distinction with the interferometric autocorrelation.

Any random noise on top of a cw signal will be identifiable in the function Ic by a small bump riding on an infinite background. The width of the bump is a measure of the temporal width of the fluctuations, and the contrast ratio (peak-to-background ratio of Ic) is a measure of the modulation depth. A 100% modulation depth results in a peak-to-background ratio of 2 to 1 for

Ic.[19]

Any signal of a finite duration results in a function Ic of finite width. If that signal has some fine structure (amplified modulation, noise) a narrow spike will appear in the middle of the correlation function. This is the coherence spike, typical of a signal consisting of a burst of noise.[19,23]

An autocorrelation free of coherence spike is a necessary condition for a coherent pulse. However, it is not a sufficient condition. A white light incoherent pulse (free of amplitude modulation) will have an autocorrelation Ic without coherence spike. That is also the case of a pulse with random or well-defined phase modulation.

IV. Characterization of Pulses by Interferometric Autocorrelations

If the measurement sketched in Fig. 3 is performed with interferometric accuracy, the second harmonic recording is proportional to the development of

$$I_t = \int |\{\mathcal{E}(t) \exp i(\omega t + \phi) + \mathcal{E}(t-\tau) \exp i[\omega(t-\tau) + \phi(t-\tau)]\}^2|^2 dt. \quad (3)$$

At zero delay the signal, being a coherent superposition of the field $\mathcal{E}$ from each arm, is

$$I_t(0) = 2^4 \int \mathcal{E}^4(t) dt. \quad (4)$$

At the next delay increment of one-half light period, the two fields add with opposite phase resulting in a near-zero signal (Fig. 4). The envelope of the constructive and destructive interferences will merge into the intensity autocorrelation for delays exceeding the pulse coherence time. Since it involves the fourth power of the fields combining in phase, the upper envelope will be more sensitive to the pulse shape than the intensity autocorrelation. The interferometric autocorrelation can provide very useful information about pulse chirp, because various types of chirps have characteristic signatures. Let us consider the interferometric autocorrelation of a pulse that has been chirped by self-phase modulation (for example, by propagation through a Kerrlike nonlinearity). Because of the frequency sweep that is largest in the center of the pulse, there will be a narrowing of the upper and lower envelopes. However, since the pulse tail and pulse front remain coherent with each other, the interferences in the wings of the interferometric autocorrelation will extend to delays as large as those for an unchirped pulse of the same duration. In the case of self-phase modulation, the narrowing of the upper and lower envelopes is a much more sensitive indication of phase modulation than the spectral broadening. Indeed, in the case of a Gaussian pulse with self-phase modulation ($\phi\alpha$ I), a chirp that reduces the interferometric autocorrelation width to 2/3 of its value (for unchirped pulses) broadens the spectrum by only 10%.

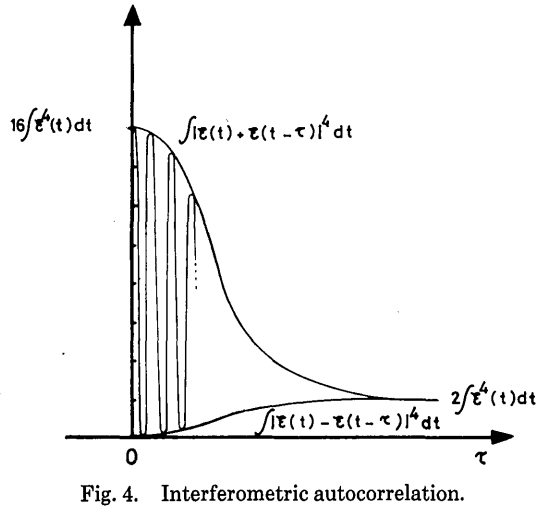

Fig. 4. Interferometric autocorrelation.

Another typical phase modulation is that caused by a linear chirp. The case of linearly chirped Gaussian pulses is discussed in the next section.

V. Linearly Chirped Gaussian Pulses

Let us consider the case of Gaussian shaped pulses with linear chirp:

$$E(t) = \exp\left\{-\left(\frac{t}{w}\right)^2 (1 + iA)\right\}. \quad (5)$$

The interferometric autocorrelation is given by

$$I_t = \left\{1 + 2\exp(-\tau^2) + 4\exp\left(-\frac{A^2+3\tau^2}{4}\right)\cos\frac{A\tau^2}{2}\cos\omega\tau + \exp[-(1+A^2)\tau^2]\cos 2\omega\tau\right\}. \quad (6)$$

The upper and lower envelopes can be found by replacing $\omega\tau$ by π or 2π in Eq. (6). For $A \neq 0$, the first derivative (with respect to τ) of the equation for the lower envelope has a zero for finite $\tau = \tau_c$ corresponding to a maximum of the lower envelope. This maximum has been calculated for various values of A and reported in Fig. 5. The maxima of the lower envelope of the interferometric autocorrelation recedes toward zero delay along a curve close to the intensity autocorrelation as the chirp parameter A is increased. In the case of a large phase modulation ($A \gg 1$), the pulse front and pulse tail are no longer coherent with each other and can no longer interfere. Therefore, the envelopes of the interferometric autocorrelation merge with the intensity autocorrelation for $\tau > \tau_c$.

A linear chirp can be induced on Gaussian pulses by propagation through dispersive media. Identification of a measured autocorrelation with Fig. 5 can be used to measure the chirp parameter A (from the height of the lower envelope maxima) as well as the pulse duration (position of the maximum). (An example of measurement of a linearly chirped pulse through its interferometric autocorrelation is presented in Sec. VIII.) The position of the maximum of the lower envelope thus provides a convenient measure of the coherence time of the pulses discussed in this section. It should be noted that this definition applies only to linearly chirped pulses, since not all chirps give rise to a lower envelope with maxima at finite delays. Mea-

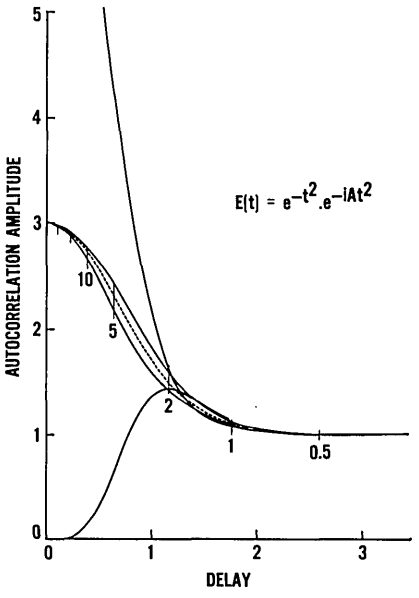

Fig. 5. Locus of the maxima of the lower envelope of the interferometric autocorrelations of linearly chirped Gaussian pulses as a function of chirp parameter A. The locus of the corresponding value of the upper envelope is also plotted. The locus of the lower envelope is only slightly below (of the upper envelope slightly above) the intensity autocorrelation (dashed line). The loci are graduated in values of chirp parameter A. The particular interferometric autocorrelation corresponding to $A = 2$ is also shown.

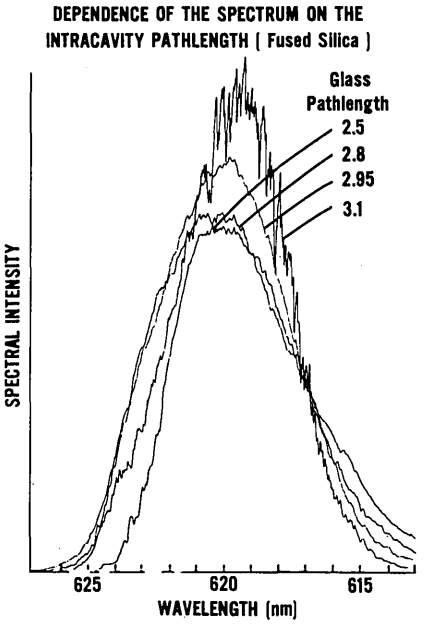

Fig. 6. Pulse spectra taken for increasing amounts of intracavity glass.

Table I. Diagnostic Functions Corresponding to Various Pulse Shapes

I(t)	Δt	I(ω)	$\Delta\omega$	$\Delta\omega/\Delta t$	$g_1(\tau)$	$\Delta\tau$	$\Delta\tau/\Delta t$	$G_2(\tau)$	$\Delta\tau$	$\Delta\tau/\Delta t$	$g_2(\tau)$
e^{-t^2}	1.665	$e^{-\omega^2}$	1.665	2.772	$1 + e^{-\frac{\tau^2}{4}}$	3.330	2	$e^{-\frac{\tau^2}{2}}$	2.355	1.414	$1 + 3G_2(\tau) \pm 4e^{-\frac{3}{8}\tau^2}$
$\mathrm{sech}^2 t$	1.763	$\mathrm{sech}^2\frac{\pi\omega}{2}$	1.122	1.978	$1 \pm \frac{\tau}{\sinh\tau}$	4.355	2.470	$\frac{3(\tau\cosh\tau - \sinh\tau)}{\sinh^3\tau}$	2.720	1.543	$1 + 3G_2(\tau) \pm \frac{3(\sinh 2\tau - 2\tau)}{\sinh^3\tau}$
$\frac{1}{(e^{\frac{t}{\sqrt{1+A}}} + e^{-\frac{t}{\sqrt{1-A}}})^2}$ $A = \frac{1}{4}$	1.715	$\frac{1 + 1/\sqrt{2}}{\cosh\frac{15\pi}{16}\omega + 1/\sqrt{2}}$	1.123	1.925	$1 \pm 4\frac{\sinh\frac{1}{3}\tau}{\sinh\frac{4}{3}\tau}$	3.405	1.985	$\frac{1}{\cosh^3\frac{8}{15}\tau}$	2.648	1.544	$1 + 3G_2(\tau) \pm 4\frac{\cosh^3\frac{4}{15}\tau}{\cosh^3\frac{8}{15}\tau}$
$A = \frac{1}{2}$	1.565	$\mathrm{sech}\frac{3\pi}{4}\omega$	1.118	1.749	$1 \pm 2\frac{\sinh\tau}{\sinh 2\tau}$	2.634	1.683	$\frac{3\sinh\frac{8}{3}\tau - 8\tau}{4\sinh^3\frac{4}{3}\tau}$	2.424	1.549	$\frac{1 + 3G_2(\tau)}{\pm 4\,\tau\cosh 2\tau - \frac{3}{2}\cosh 2\frac{2}{3}\tau\sinh\frac{2}{3}\tau(2 - \cosh\frac{4}{3}\tau)}{\sinh^3\frac{4}{3}\tau}$
$A = \frac{3}{4}$	1.278	$\frac{1 - 1/\sqrt{2}}{\cosh\frac{7\pi}{16}\omega - 1/\sqrt{2}}$	1.088	1.391	$1 \pm \frac{4\sinh 3\tau}{3\sinh 4\tau}$	1.957	1.531	$\frac{2\cosh\frac{16}{7}\tau + 3}{5\cosh^3\frac{8}{7}\tau}$	2.007	1.570	$1 + 3G_2(\tau) \pm 4\frac{\cosh^3\frac{4}{7}\tau\,(6\cosh\frac{8}{7}\tau - 1)}{5\cosh^3\frac{8}{7}\tau}$
$\frac{1}{(e^t + e^{-rt})^2}$		$\frac{2(1-y)x}{x^2 - 2yx + 1}$ where, $x = \exp(\frac{2\pi\omega}{1+r})$ $y = \cos(\frac{2\pi r}{1+r})$			$1 \pm \frac{r+1}{r-1}\frac{\sinh(\frac{r-1}{2}\tau)}{\sinh(\frac{r+1}{2}\tau)}$						

I(t) and I(ω) are the intensities in the time and (angular) frequency domains, respectively. $g_1(\tau)$ is the first-order autocorrelation of the field envelope. $G_2(\tau)$ is the intensity autocorrelation, and $g_2(\tau)$ the envelope of the interferometric autocorrelation. The FWHM is indicated in the next column to the right for each function.

surement of an interferometric autocorrelation with an envelope matching that of Eq. (6) does not unambiguously indicate a linearly chirped Gaussian pulse. The measurements are always an average over a large number of pulses. The effect of a statistical distribution of pulse durations on the intensity autocorrelation has been considered by Van Stryland.[24] In the latter paper, it was shown that the intensity autocorrelation for a series of Gaussian pulses statistically distributed in pulse width has exponential wings. Such a shape could also be interpreted as the intensity autocorrelation of identical single-sided exponential pulses. Intensity autocorrelations with exponential wings are quite often observed with synchronously pumped lasers. A recent theory by Catherall and New[25] indicates that indeed one expects a jitter in pulse duration for this type of laser. A similar type of ambiguity exists for the phase function. The interferometric autocorrelations for a train of unchirped Gaussian pulses, with a frequency distribution $F(\Delta\omega)$ around a central frequency ω_0 [$\omega = \omega_0 + \Delta\omega$], is

$$I_t = \{1 + 2\exp(-\tau)^2) + 4\exp(-3/4\tau^2)\cos\omega\tau + \exp(-\tau^2)\cos 2\omega\tau\}F(\Delta\omega). \quad (7)$$

In the small chirp limit ($\cos A\tau^2/2 \cong 1$), Eq. (7) is identical to the expression of Eq. (6) for

$$F(\Delta\omega) = \frac{\sqrt{2}}{A}\exp\left(-\frac{\Delta\omega^2}{A^2}\right). \quad (8)$$

A train of Gaussian pulses with a Gaussian distribution of frequencies has thus the same interferometric autocorrelation as a linearly chirped Gaussian pulse. Several other types of measurement have to be done to ensure that the laser output consists of a train of identical pulses. In the case of the laser used in this work, the pulse-to-pulse reproducibility in shape and frequency has been verified by the following criteria:

(a) no fluctuation in pulse energy as measured in real time by a fast photodiode nor in the energy of the second harmonic;

(b) the spectrum of the second harmonic corresponds to the square of that of the fundamental (Sec. X);

(c) overall agreement of the fitting of linear (spectrum) and nonlinear (correlation) measurements; and

(d) the pulse compression and broadening observed by propagation through glass is consistent with the chirp (and shape) determination through the method detailed in Sec. VIII.

VI. Analytical Autocorrelation Functions for Selected Pulse Shapes

The process of pulse shape identification is greatly simplified if a set of typical test functions is available. We have found analytical solutions for the measurements associated with the most common pulse shape functions encountered. For the sake of completeness, we have included the linear autocorrelation $g_1(\tau)$ defined as

$$g_1(\tau) = \int_{-\infty}^{\infty} |E(t) + E(t-\tau)|^2 dt / 2 \int |E(t)|^2 dt. \quad (9)$$

Since the Fourier transform of the first-order autocorrelation $g_1(\tau)$ is equal to $I(\omega) + I(-\omega)$ [where $I(\omega)$ is the pulse spectral intensity], it does not contain more information than the spectrum. The normalized second-order interferometric autocorrelation $g_2(\tau)$ is defined by

$$g_2(\tau) = \int_{-\infty}^{\infty} |\{E(t) + E(t-\tau)\}^2|^2 dt / 2 \int_{-\infty}^{\infty} |E^2(t)|^2 dt. \quad (10)$$

The fringe averaged portion of $g_2(\tau)$ is the intensity autocorrelation $G_2(\tau)$:

$$G_2(\tau) = \int_{-\infty}^{\infty} |E^2(t)E^2(t-\tau)| dt / \int_{-\infty}^{\infty} |E^2(t)|^2 dt. \quad (11)$$

The spectral intensity $I(\omega)$, the first-order [$g_1(\tau)$], and second-order [$g_2(\tau)$] autocorrelations are listed in Table I for various pulse shapes. The FWHM of the corresponding functions is indicated. For Gaussian pulses the integrations can be performed simply by the method of completing squares. For pulse shapes of the form $\mathcal{E}(t) = 1/\{\exp[t/(1+A)]\exp[-t/(1-A)]\}$, the integrals involved in the development of the second-order autocorrelation can be obtained by the method of partial fractions. For the more general case $\mathcal{E}(t) = 1/\{\exp(rt + \exp(-rt)\}$, where r is any real number, the integrals are obtained by contour integration. The contour is the same as that used to calculate the Fourier transform of a sech shaped envelope.[26] The autocorrelations of the functions listed in Table I can also be calculated for linearly chirped pulses. However, the expressions become too complex to be useful in view of the availability of a more practical numerical alternative discussed in Sec. VII.

VII. Determination of the Shapes—in Amplitude and Phase—of the Pulses Produced by the Laser

The pulse shape—in amplitude and phase—is determined from simultaneous fitting of the intensity, interferometric autocorrelations, and spectrum. The case of arbitrary shape and/or nonlinear chirp cannot be handled by the analytical expressions given in the previous section. Instead, we developed a computer program to generate the spectrum and correlations for an arbitrary input pulse. It should be noted that, for strongly phase modulated pulses, the interferometric autocorrelation is also chirped. Therefore, each point of the upper or lower envelope has to be calculated by seeking the maximum (or minimum) of each individual fringe. The pulse is Fourier transformed to calculate the effect of dispersion through the excess glass (of one arm of the interferometer), thereafter transformed back into the time domain to calculate the (interferometric and intensity) cross correlation with the original pulse. The use of the intensity autocorrelation alone as proposed by Anderson and Eng[27] does not remove two major uncertainties. Because the second-order autocorrelations are symmetric (except for the eventual effect of pulse dispersion in the beam splitter of the autocorrelator) the same autocorrelation function can represent a symmetrical or an asymmetrical pulse. The ambiguity is replaced by an assumption of minimum phase in Ref. 27, which cannot be verified independently for the pulses produced by the laser. The second

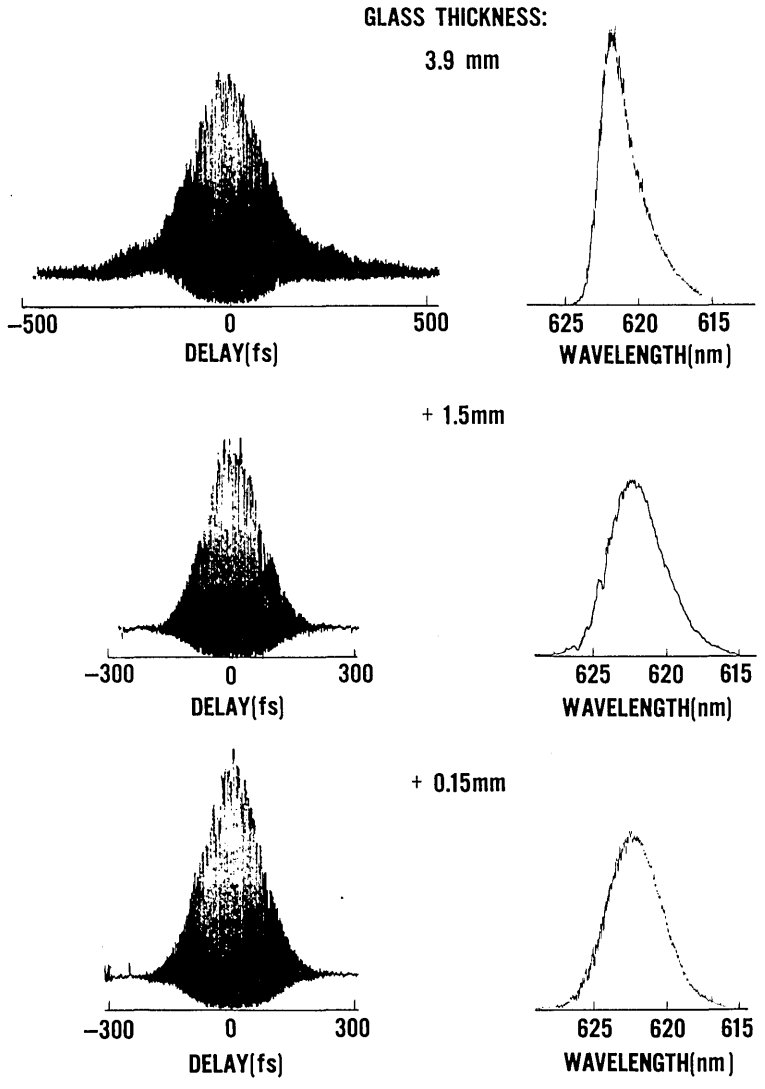

Fig. 7. Three successive spectra and corresponding interferometric autocorrelations taken for successive increments of intracavity glass (indicated in the figure).

unknown is the phase of the pulse electric field, on which no information is contained in the intensity autocorrelation.

The evolution of pulse spectra with an increasing amount of intracavity glass is illustrated in Fig. 6. The spectrum is asymmetric, with a sharp edge on the long-wavelength side, for less glass than optimum in the cavity. As the fused silica prism is translated to increase the amount of intracavity glass, the spectrum becomes symmetric as the pulse duration passes through a minimum. For an overcompensated cavity (more glass than optimum), the spectrum has reversed symmetry: the sharp edge is on the short-wavelength side. The amount of intracavity glass has to be adjusted quite accurately in order to reach perfect chirp compensation (minimum pulse duration and symmetric spectrum). The pulse spectrum is seen to reverse symmetry between 2.8 and 2.95 mm of glass in Fig. 6.

A similar evolution of interferometric autocorrelations is shown next to that of pulse spectra for three different glass thicknesses in Fig. 7. For a cavity undercompensated by 2.5 mm (glass thickness 3.9 mm), the interferometric autocorrelation has a shape typical of nonlinear chirp. The interference region extends in the wings, because the pulse front and tail are not frequency modulated, and are thus coherent with each other. The maximum chirp occurring near the center of the pulse narrows the central portion of the autocorrelation. As optimal compensation is approached (middle and lower parts of Fig. 7), the spectrum becomes symmetric, and the interferometric autocorrelation takes the characteristics shape (sharp transition from the interference region to the uniform background at 1/8 peak height) of an unchirped pulse.

The phase modulation is primarily induced by off-resonance saturation in DODCI. Moving the absorber dye jet out of the focal spot results in a strong decrease in glass thickness required for optimum chirp compensation.[12,17] The magnitude and sign of the nonlinear chirp agrees with the recent theoretical calculations of Rudolph and Wilhelmi.[11] In addition to the nonlinear chirp induced by self-phase modulation, the

cavity length dispersion effect (resulting from a nonzero $d^2P/d\lambda^2$ where P is the cavity perimeter) calculated by Gordon and Fork[16] adds a linear contribution to the downchirp. The strong dependence of optimum glass thickness on the intensity in the absorber[12,17] indicates that self-phase modulation is dominant but does not provide a way to quantitatively isolate one effect from the other.

One might wonder how a nonlinear chirp can be compensated through linear dispersion of glass in this laser. The theories of Diels *et al.*,[14,17] Dietel *et al.*,[28] and Rudolph and Wilhelmi[11] predict an unchirp of the leading edge of the pulse. The unchirped part of the pulse will be broadened by passage through the glass. Since this broadened weaker signal is ahead of the pulse, it will be attenuated in the absorber and eventually vanish. As the compensation increases, the upchirped parts of the pulse subside in the cavity, and only the downchirped part remains. At optimum chirp compensation, the cycling of the pulses through the cavity can be described as a solution propagating in an infinite medium with a distributed gain–loss function equivalent to one cycle through the cavity.[14,17,28]

At optimum chirp compensation, the symmetric spectrum and the autocorrelations can easily be fit with an unmodulated pulse of shape

$$\mathcal{E}(t) = \frac{1}{\exp(t/\tau_F) + \exp(-t/\tau_R)}, \tag{12}$$

with $\tau_F/\tau_R \cong 0.7/1.3$. The preferred mode of operation however is with a slightly undercompensated downchirp for which the nonlinearity of the phase modulation is still negligible and the laser stability is optimal. The corresponding interferometric autocorrelation is displayed in Fig. 8. The slight departure of the 8/1 ratio results from a small imbalance of the losses in the two arms of the autocorrelator—an effect that has been corrected for in the fitting summarized by the sequence of Fig. 9. The experimental data [intensity autocorrelation, Fig. 9(a); spectrum, Fig. 9(b); and envelopes of the interferometric autocorrelations, Fig. 9(c)] are reported as crosses in Fig. 9, while the solid lines are the calculated functions for the trial pulse shape:

$$\mathcal{E}(t) = \exp[-0.15i(t/\tau)^2]/\{\exp[-t/0.75\tau] + \exp[t/1.25\tau]\}. \tag{13}$$

In Eq. (13), $\tau = 44$ fsec and the pulse duration (FWHM of the intensity) is 76 fsec ($=1.72\tau$). The accuracy of the fitting of first-order (spectrum) as well as second-order (autocorrelations) measurements is an indication that there are no pulse-to-pulse fluctuations. A more rigorous demonstration that pulse averaging effects are negligible in this laser is contained in a comparison of the spectrum of the pulse train with that of the second harmonic given in Sec. X.

It should be noted that this slightly downchirped pulse represents a best mode of operation of the laser for the following reasons. A slight downchirp is desirable in order to compensate pulse broadening through dispersion that is inevitable in the optical components (windows, mirrors). The small downchirp near optimum chirp compensation can be assimilated to a linear phase modulation. With slightly more (of the order of tens of microns) intracavity glass, shorter pulses can be generated but at the expense of a decrease in stability.

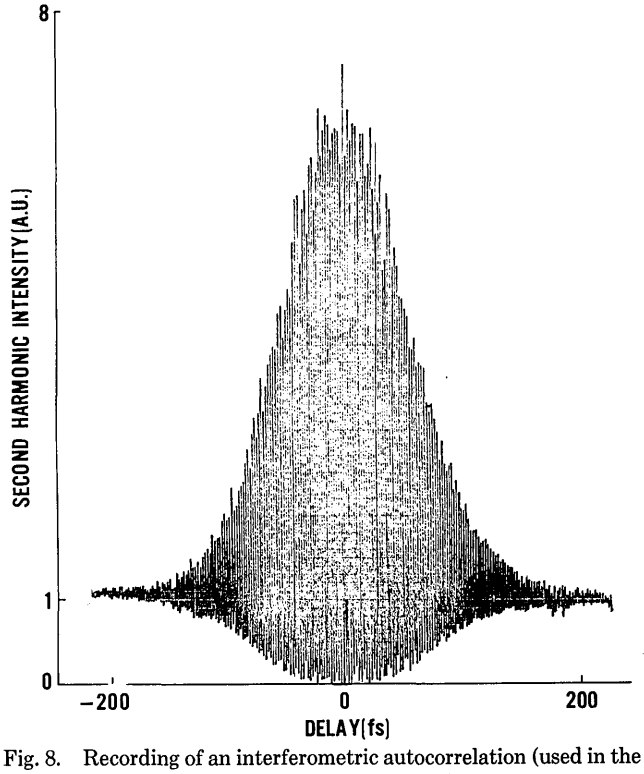

Fig. 8. Recording of an interferometric autocorrelation (used in the pulse shape fitting of Fig. 9).

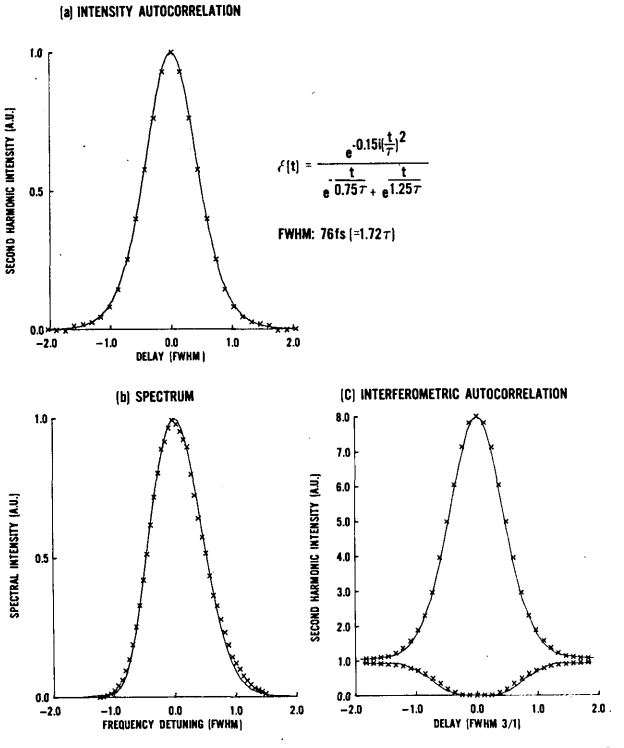

Fig. 9. Example of pulse shape determination through fitting of the intensity autocorrelation (a), the pulse spectrum (b), and the interferometric autocorrelation (c). The crosses are the experimental data points. The solid lines are the corresponding functions calculated for the trial test function indicated in the figure.

The low frequency noise increases and the mode-locked operation becomes more sensitive to the alignment and position of jet. Therefore, in experiments requiring a high temporal resolution[29] a higher accuracy and higher signal-to-noise can often be obtained using slightly downchirped pulses, 20–50% longer than the minimum pulse duration obtainable from the laser. A precise pulse shape determination as illustrated in Fig. 9 ensures a better temporal resolution than would be obtained with shorter, less stable pulses.

VIII. Pulse Compression and Broadening in Glass

The propagation of initially bandwidth-limited pulses (i.e., without phase modulation) through normally dispersive media (for example, glass) is a classical problem of propagation that can be solved analytically for pulses with a Gaussian temporal profile within the approximation of negligible pulse distortion. After propagation through a thickness L of glass, an initially unchirped pulse $E = E_1 \exp - (t/\tau_1)^2$ becomes $E = E_2 \exp - (t/\tau_2)^2[1 + iA]$ with a broadening given by[30]

$$\tau_2 = \tau_1 \sqrt{1 + k_0^2}, \tag{14}$$

and a linear chirp parameter

$$A = k_0. \tag{15}$$

The parameter k_0 characterizing the pulse distortion is the second derivative of the phase change (by transmission) with respect to the frequency normalized to the inverse pulse width:

$$k_0 = 2\frac{d^2\phi}{d(\omega\tau_1)^2} = \frac{2}{\tau_1^2}\cdot\frac{d^2k}{d\omega^2}, \tag{16}$$

where

$$\frac{d^2k}{d\omega^2} = \frac{2}{c_0}\frac{dn}{d\omega} + \frac{\omega}{c_0}\frac{d^2n}{d\omega^2}. \tag{17}$$

In Eq. (16), c_0 is the speed of light in vacuum, L the thickness, and n the index of refraction of glass.

We have performed measurements of broadening in two types of glass: SF5 and BK7. For these two types of glass, a cubic fit of the published data on the index of refraction[31] around 625 nm gives

$$n_{SF5} = 1.6691 + 0.1792 \times 10^{-3}\,\Delta\omega + 0.3743 \times 10^{-6}\,\Delta\omega^2 + 0.38 \times 10^{-8}\,\Delta\omega^3,$$

and

$$k(\Delta\omega) = 0.9735 \times 10^{-2}\,\Delta\omega^2 + 0.5124 \times 10^{-4}\,\Delta\omega^3. \tag{18}$$

$$n_{BK7} = 1.5153 + 0.7326 \times 10^{-4}\,\Delta\omega + 0.8772 \times 10^{-7}\,\Delta\omega^2 + 0.16 \times 10^{-8}\,\Delta\omega^3,$$

and

$$k(\Delta\omega) = 0.3323 \times 10^{-2}\,\Delta\omega^2 + 0.1907 \times 10^{-4}\,\Delta\omega^3. \tag{19}$$

In Eq. (18) and (19), $\Delta\omega$ is the frequency measured from the central pulse frequency ($\Delta\omega = \omega - \omega_c$ where $\omega_c = 2\pi/c/\lambda_0$ where $\lambda_0 = 625$ nm) in units of 10^{-13} sec^{-1}, while the correction to the wave vector $k(\Delta\omega)$ (of order larger than 1 in $\Delta\omega$) is in mm^{-1}.

Since the results are qualitatively identical for both types of glass, we will discuss here only the more dispersive results obtained with SF5 glass. For a 90-fsec pulse propagating through 100 mm of SF5 glass, the linear chirp parameter [from Eqs. (19) and (17)] is $k_0 = 4.8$, and the broadening factor $\sqrt{(1 + k_0^2)} = 5$. Thus we expect from the Gaussian theory that the 90-fsec pulse broadens to 450 fsec, while the intensity autocorrelation of the transmitted pulse indicates a broadening to only 350 fsec (assuming Gaussian pulse shape). A quick estimate for the chirp can be extracted from the experimental interferometric autocorrelation with the help of Fig. 5. We find a value of the chirp parameter of 6.3 against 4.8 for the value deduced from the linear dispersion theory. All these discrepancies are another indication that the pulse shape is too far from a Gaussian for the classical broadening by dispersion formula (16) to apply. A numerical analysis based on the experimentally determined pulse shape gives a consistent picture, as shown below.

The best fit of the autocorrelation and spectra for the initial pulse is for the pulse

$$E(t) = \frac{\exp[-iA(t/\tau)^2]}{\exp[t/\tau(1 + a)] + \exp[-t/\tau(1 - a)]}, \tag{20}$$

with $\tau = 120$ fsec, an asymmetry characterized by $a = 0.75$, and a chirp parameter of $A = 0.25$. The intensity autocorrelation of this pulse has a FWHM of 130 fsec. The FWHM of the pulse itself is 87 fsec. We calculated the transmitted pulse through a thickness d of glass by computing the Fourier transform of the pulse (20), multiplying it by the phase factor $\exp[-ik(\Delta\omega)d]$. The FWHM of the transmitted pulse is 390 fsec. The FWHM of the intensity autocorrelation of the transmitted pulse is 570 fsec, indicating a broadening by a factor of 4.38. This is in excellent agreement with the measured broadening of a factor 4.3 ± 0.2.

A comparison of the calculated (solid line) vs measured interferometric autocorrelation of the transmitted pulse is shown in Fig. 10. There is no adjustable parameter in the computation leading to the solid line, since the input pulse shape [Eq. (20)], chirp, and duration were derived directly from the (input) data for the laser pulses. While the input pulse had a slight down-

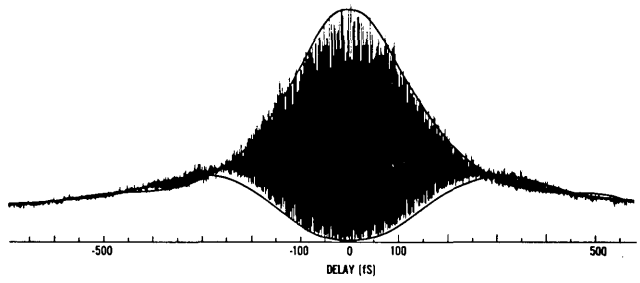

Fig. 10. Interferometric autocorrelation of a pulse that propagated through 10 cm of SF5 glass. The solid line is a calculated autocorrelation using published data on SF5 to calculate the distortion of the initial pulse shape. The latter (detailed in the text) was determined by simultaneous fitting of the autocorrelations and spectrum.

chirp, the transmitted pulse has an upchirp of 57×10^{24} sec^{-2}. It is interesting to compare this value of the chirp with the estimate obtained from Fig. 5. The phase modulation corresponding to a linear chirp of 57×10^{24} sec^{-2} is $A(t/\tau_g)^2$, with $A = 6$ and $\tau_g = 460$ fsec is the $1/e$ HW of the Gaussian pulse with the same FWHM as the transmitted pulse (390 fsec). Reporting the ratio of the maximum of the lower envelope to the peak of the autocorrelation of Fig. 10, in Fig. 5 we find a chirp coefficient of $A = 6.3$. We thus conclude that, even though Fig. 5 was calculated for a Gaussian shape, the ordinate of the maximum of the lower envelope of the interferometric autocorrelation provides a quick and accurate measure of the linear chirp of a pulse (even an asymmetric one).

As noted previously, the effect of normal dispersion of optical components on femtosecond pulses can be partly compensated by using downchirped pulses. The laser is operated with less intracavity glass, to produce longer downchirped pulses, which are then compressed extracavity by propagation through glass. However, since linear propagation through transparent media does not modify the pulse spectrum, the latter process is much less efficient than intracavity compression. Indeed, even in the case of a linearly downchirped asymmetric pulse, the spectrum is asymmetric and cannot represent the Fourier transform of a real function. The extracavity pulse compression will be even less effective for strongly undercompensated cavities, which produce pulses with a nonlinear chirp. The effectiveness of extracavity pulse compression compared to intracavity chirp compensation is illustrated in Fig. 11. The pulse duration is plotted as a function of extracavity glass (BK7) thickness. In the top figure, the laser is undercompensated by 1 mm of intracavity glass—in this case the intracavity prism was made of fused silica. A longer pulse duration is measured after compression through 100 mm of BK7 glass than the minimum duration obtained with the exactly compensated cavity (3.2-mm intracavity glass). The lower portion of the figure uses a more strongly chirped pulse, generated with the laser undercompensated by 2.2 mm of fused silica (the laser cavity alignment was slightly modified to have a larger self-phase modulation requiring 9 mm of intracavity fused silica for optimum compensation). The difference between minimum pulse durations obtained by extracavity vs intracavity compression is 2.5 times larger than in the previous case.

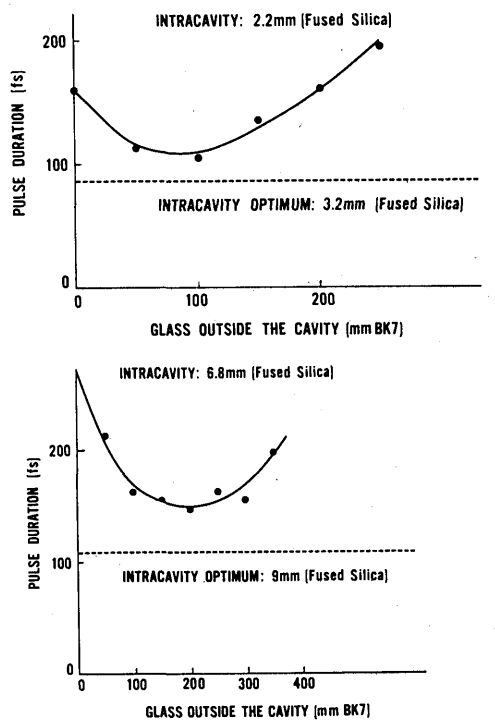

Fig. 11. Extracavity chirp compensation. The laser is undercompensated by 1 mm (above) or 2.2 mm (below) of fused silica. The pulse duration is measured after transmission through various thicknesses of BK7 glass.

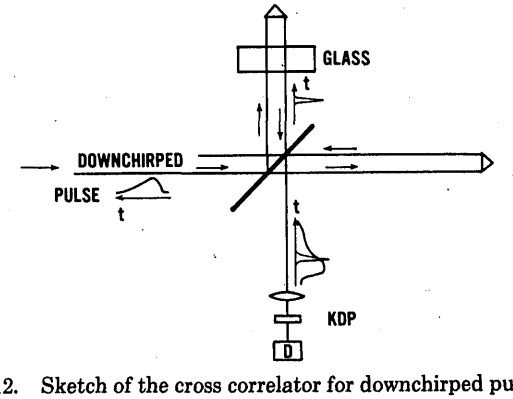

Fig. 12. Sketch of the cross correlator for downchirped pulses. A block of glass (5 cm of BK7) is inserted in one arm of the interferometer. As the delay in that arm is varied, the cross correlation of the original pulse with the pulse compressed through the glass will be measured.

IX. Direct Measurement of the Shape of Downchirped Pulses

Downchirped pulses can be compressed (by as much as a factor of 2 in the case of the lower portion of Fig. 11) by simply propagating them through a block of glass. This offers a possibility to observe directly their shape by inserting the appropriate thickness of glass in one arm of the autocorrelator, as sketched in Fig. 12. After passage through glass, the downchirped pulse is compressed. As one leg of the interferometer is translated, the second harmonic signal is proportional to the cross correlation of the compressed pulse with the original one.

For the measurement reported in Fig. 12, a block of 5-cm BK7 glass was inserted in one arm of the interferometer. The successive autocorrelations of Fig. 12 show, from top to bottom, the downchirped pulse from the laser, the pulse after propagation through 10 cm of BK7 glass, and the result of the cross correlation with 5-cm BK7 inserted in one arm of the interferometer. The interferometric autocorrelation of the laser pulse (top of the figure) is typical of a nonlinear phase modulation.

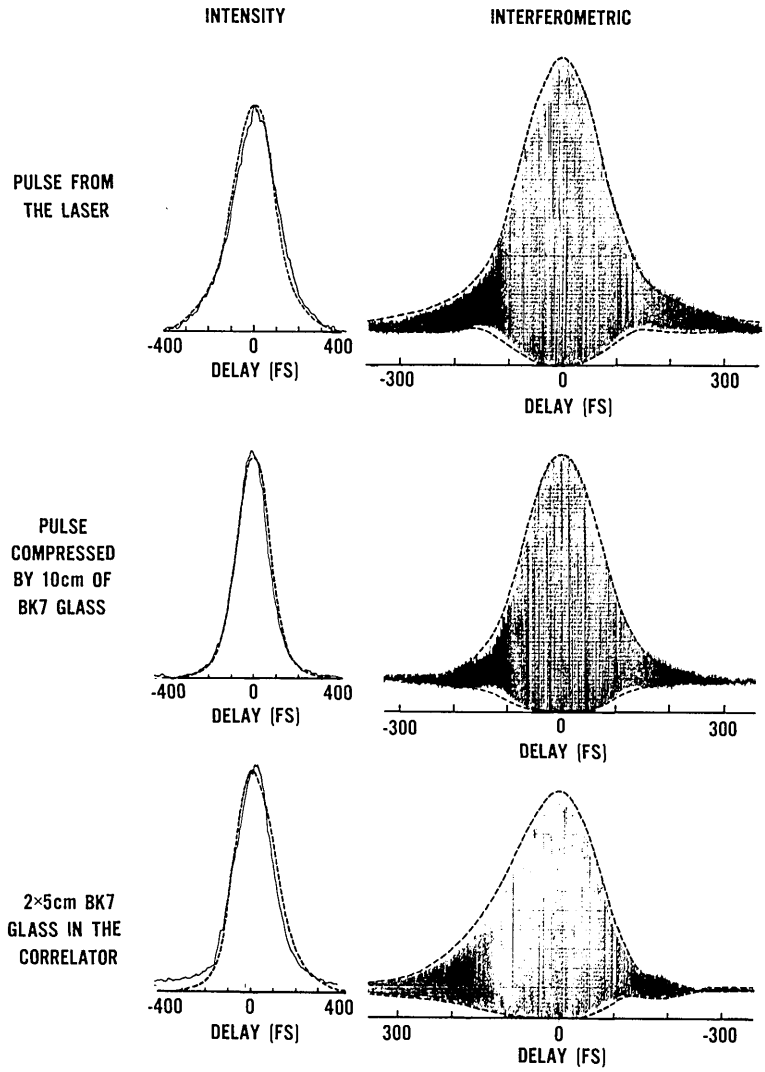

Fig. 13. Above: intensity and interferometric autocorrelations of the laser pulse. These measurements, together with the pulse spectrum, were used to determine the pulse shape and chirp. The dashed line is the result of the fitting procedure for the pulse electric field envelope indicated in the text. Middle: intensity and interferometric autocorrelations of the pulse after propagation through 10 cm of BK7 glass. The dashed lines are obtained by calculating successively the propagation and autocorrelations of the laser pulse determined from the previous fitting. Below: intensity and interferometric correlations after insertion of 5-cm BK7 glass in one arm of the interferometer of Fig. 12. The dashed lines are calculated correlations using the laser pulse shape determination of the upper figure.

There is no straightforward method to determine the shape and phase modulation of a pulse with a nonlinear chirp as produced by the laser with little or no chirp compensation. The fitting procedure outlined in Sec. VII can still be applied. The theory of the passively mode-locked dye laser[11,17] facilitates the fitting procedure by providing a reasonable starting point for the first iteration. Indeed, it has been shown[11,17] that the frequency modulation induced by transmission through the saturable absorber has a similar temporal dependence as the pulse intensity and reaches its peak value one pulse width (FWHM of the intensity) ahead of the peak of the pulse. A linear chirp is added to the nonlinear one to account for the dispersion of the various (linear) intracavity components. We find a best fit for the following pulse shape:

$$E(t) = \frac{\exp[i\phi(t)]}{\exp[-t/\tau(1-a] + \exp[t/\tau(1+a)]}, \tag{21}$$

with

$$\phi = \int \frac{2Bdt/\tau}{\exp(-t_R) + \exp(t_F)} + A(t/\tau)^2. \tag{22}$$

The rise and fall of the frequency modulation are characterized by

$$t_R = 2(t - t_c)/\tau(1-a), \qquad t_F = 2(t - t_c)/\tau(1+a).$$

The values of the various parameters (obtained by fitting successively the pulse spectrum, intensity, and interferometric autocorrelation) are

pulse asymmetry:	a	$= 0.55$
nonlinear chirp;	B	$= 2.3$
linear chirp:	A	$= -0.2$

offset of the frequency modulation:	t_c/τ	= 1.
pulse duration:	τ	= 88 fsec, which results in a pulse duration

(FWHM of the intensity) of 135 fsec.

The intensity and interferometric autocorrelations calculated for this pulse shape are indicated by the dotted line (top of Fig. 13). The data are represented by the solid lines. As in the previous section, we calculate the transmission through 10 cm of BK7 by Fourier transforming the pulse complex envelope and multiplying it by the appropriate phase factor before retransforming it back into the time domain. Next, the transmitted pulse is correlated with itself (middle of Fig. 13) and with the initial pulse (bottom of Fig. 13). The dotted lines show the calculated functions, while the solid lines show the experimental data. Only the data of the upper figure were used to determine the pulse shape. The calculated curves for the middle and lower part of the figure were obtained without the use of any adjustable parameter. Comparison between the theoretical and experimental cross correlation could be used to improve the pulse shape fit. Because of the initial downchirp, the pulse transmitted through the glass is 1.8 times shorter than the initial one. Hence, the cross correlations exhibit the asymmetry in shape and chirp of the laser pulse (and provide independent confirmation that indeed it is the rise time that is shorter than the fall time). Because of the nonlinear frequency modulation of the laser pulse, the pulse transmitted through glass has an interesting shape, with a relatively slow rise ($1/e$ of max rise time = 120 fsec) and a steep decay ($1/e$ of max fall time = 82 fsec).

X. Bandwidth of the Second Harmonic

Two fundamental field (centered around the laser frequency ω) envelopes E_1 and E_2 combine in the nonlinear crystal to generate the second harmonic:

$$E_{2\omega} = \eta(\omega)E_1E_2. \tag{23}$$

The conversion efficiency $\eta(\omega)$ will, in general, be different for various frequency components of the pulse for which the phase of the fundamental and second harmonic are not matched over the entire crystal length. Fourier transforming (23) yields

$$E_{2\omega}(\tau) = \int dt \int dt' \eta(t')E_1(t' - t)E_2(t - \tau)dt. \tag{24}$$

The expression (24) is equal to the correlation of the fields E_1 and E_2 only if the conversion efficiency is constant over the frequency range covered by $E(\omega)$ [$\eta(\omega) = \omega_0$]. If the phase matching is not uniform over the bandwidth of interest, the measured correlation functions will be broadened. It is therefore important to use a short conversion length to ensure that the phase of the second harmonic field follows that of the fundamental for the whole pulse spectrum. This can be done either by using short nonlinear crystals or tight focusing. We have used either 0.3-mm thickness KDP crystals (focusing with a 22-mm focal distance lens) or crystals of 2-mm thickness (focusing with a microscope objective with a magnificantion factor of 8×).

We have verified that the second harmonic generating crystal provides uniform conversion over a sufficient bandwidth by comparing the spectra of the second harmonic and of the fundamental. The square root of the second harmonic intensity plotted (dotted line) as a function of fundamental wavelength is seen to match accurately the pulse spectrum (Fig. 14). Such a comparison serves many purposes:

(a) to verify that the harmonic conversion does not act as a narrowband filter;

(b) to verify that pulse-to-pulse fluctuations in the train are negligible; and

(c) to verify that background radiation between pulses is negligible (indeed, since the duty cycle of the pulses is typically of 10^{-5}, continuous radiation of $1/10^5$ of the laser peak power will affect significantly the linear spectrum, while being a negligible contribution to the nonlinear spectrum.

XI. Conclusions

We have demonstrated a source capable of generating femtosecond pulses of controllable shape and chirp as well as accurate diagnostic methods to measure these parameters. Analytical expressions are derived to provide a quick identification of various typical pulse shapes through their interferometric and intensity autocorrelations as well as their spectrum. The latter functions are calculated numerically from trial functions for the fitting of more complex pulse shapes and chirp. The accuracy of the determination of the pulse amplitude and phase is demonstrated by the consistency of various measurements and calculations of pulse broadening and compression through glass.

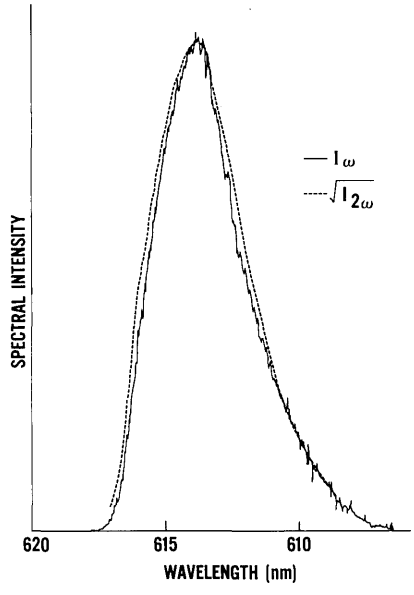

Fig. 14. Comparison of the pulse spectrum with that of the second harmonic.

The laser emission is shown to consist of a train of identical pulses of asymmetric shape with a steep rise and slower decay. The frequency modulation can be adjusted from being strongly nonlinear to a small linear downchirp and even zero modulation. A wide variety of pulse shapes can be created through a combination of chirp control and propagation through glass. It is, for example, possible to reverse the asymmetry of the source pulse (i.e., to transform it into a pulse of slow rise and steep decay).

This work was supported by the National Science Foundation under grant ECS-8406985.

References

1. R. L. Fork, B. I. Green, and C. V. Shank, "Generation of Optical Pulses Shorter than 0.1 ps by Colliding Pulse Mode-Locking," Appl. Phys. Lett. **38,** 671 (1981).
2. W. Dietel, E. Dopel, D. Kühlke, and B. Wilhelmi, "Pulses in the Femtosecond Range from a cw Dye Ring Laser in the Colliding Pulse Mode-Locking Regime with Downchirp," Opt. Commun. **43,** 433 (1982).
3. W. Dietel, J. J. Fontaine, and J.-C. Diels, "Intracavity Pulse Compression with Glass: A New Method of Generating Pulses Shorter than 60 fsec." Opt. Lett. **8,** 4 (1983).
4. J. J. Fontaine, W. Dietel, and J.-C. Diels, "Chirp in a Mode-Locked Ring Laser," IEEE J. Quantum Electron. **QE-19,** 1467 (1983).
5. J.-C. Diels, E. W. Van Stryland, and D. Gold, "Investigation of the Parameters Affecting Subpicosecond Pulse Duration of Passively Mode-Locked Dye Laser," in *Proceedings, First International Conference on Picosecond Phenomena* (Springer, New York, 1978), p. 117.
6. J.-C. Diels, J. J. Fontaine, and F. Simoni, "Phase Sensitive Measurements of fs Laser Pulses from a Ring Cavity," in *Lasers 83, San Francisco* (Dec. 1983).
7. B. Nikolaus and D. Grischowsky, "12× Pulse Compression Using Optical Fibers," Appl. Phys. Lett. **42,** 1 (1983).
8. D. Kuhlke, W. Rudolph, and B. Wilhelmi, "Calculation of the Colliding Pulse Mode Locking in cw Dye Ring Lasers," IEEE J. Quantum Electron. **QE-19,** 526 (1984).
9. W. Dietel, "Transient Absorber Gratings Shorten the Pulses of a Passively Mode-Locked cw Dye Laser," Opt. Commun. **43,** 69 (1982).
10. J.-C. Diels, I. C. McMichael, J. J. Fontaine, and C. Y. Wang, "Subpicosecond Pulse Shape Measurement and Modeling of Passively Mode Locked Dye Lasers Including Saturation and Spatial Hole Burning," in *Proceedings, Third International Conference on Picosecond Phenomena* (Springer, Berlin, 1982), p. 116.
11. W. Rudolph and B. Wilhelmi, "Calculation of Light Pulses with Chirp in Passively Mode Locked Lasers Taking into Account the Phase Memory of Absorber and Amplifier," Appl. Phys. B **34,** 274 (1984).
12. J.-C. Diels *et al.* "Control of Profile and Chirp of fs Light Pulses by Propagating Them Through Resonant and Nonresonant Optical Media," *IQEC 84, Anaheim* (June 1984), paper MDD3.
13. J.-C. Diels *et al.* "Colliding Pulse Femtosecond Lasers and Applications to the Measurement of Optical Parameters," in *Ultrafast Phenomena IV* (Springer, Berlin, 1984), pp. 30–34.
14. J.-C. Diels *et al.* Kvantovaya Elektron **10,** 2398 (1983); "Experimental and Theoretical Study of a Femtosecond Laser," Sov. J. Quantum Electron. **13,** 1562 (1983).
15. W. Dietel, E. Dopel, K. Hehl, W. Rudolph, and E. Schmidt, "Multilayer Dielectric Mirrors Generate Chirp in fs Dye Ring Lasers," Opt. Commun. **50,** 179 (1984).
16. J. P. Gordon and R. L. Fork, "Optical Resonator with Negative Dispersion," Opt. Lett. **9,** 153 (1984).
17. J.-C. Diels, J. J. Fontaine, W. Dietel, W. Rudolph, and B. Wilhelmi, "Analysis of a Mode Locked Ring Laser: Chirped Solitary Pulse Solutions," J. Opt. Soc. Am. B **2,** 680 (1985).
18. J.-C. Diels, H. Vanherzeele, and R. Torti, "Femtosecond Pulse Generation in a Linear Cavity Terminated by an Antiresonant Ring," in *Technical Digest, Conference on Lasers and Electro-Optics* (Optical Society of America, Washington, D.C., 1984), paper WC5.
19. H. P. Weber and H. G. Danielmeyer, "Multimode Effects in Intensity Correlation Measurements," Phys. Rev. A **2,** 2074 (1970).
20. K. L. Sala, G. A. Kenny-Walace, and G. E. Hall, "CW Autocorrelation Measurements of Picosecond Laser Pulses," IEEE J. Quantum Electron. **QE-16,** 990 (1980).
21. E. P. Ippen and C. V. Shank, "Techniques for Measurements," in *Ultrashort Light Pulses*, S. L. Shapiro, Ed. (Springer, New York, 1977), pp. 313–345.
22. E. P. Ippen and C. V. Shank, "Dynamic Spectroscopy and Subpicosecond Pulse Compression," Appl. Phys. Lett. **27,** 488 (1975).
23. D. J. Bradley and G. H. C. New, "Ultrashort Pulse Measurements," Proc. IEEE **62,** 313 (1974).
24. E. W. Van Stryland, "The Effect of Pulse to Pulse Variation on Ultrashort Pulsewidth Measurements," Opt. Commun. **31,** 93 (1979).
25. J. M. Catherall and G. H. C. New, "Theoretical Studies of Active, Synchronous, and Hybrid Mode-Locking," in *Ultrafast Phenomena IV* (Springer, Berlin, 1984), pp. 75–77.
26. G. Arfkin, *Mathematical Methods for Physicists* (Academic, New York, 1970).
27. T. Anderson and S. T. Eng. "Determination of the Pulse Response from Intensity Autocorrelation Measurements of Ultrashort Laser Pulses," Opt. Commun. **47,** 288 (1983).
28. W. Dietel, W. Rudolph, B. Wilhelmi, J.-C. Diels, and J. J. Fontaine, "Formation of Solitary Femtosecond Light Pulses with Chirp in Passively Mode Locked Lasers," in *Conference on Ultrafast Phenomena in Spectroscopy*, Minsk (1983); Izv. Akad. Nauk SSSR Ser. Fiz. **48,** 480 (1984).
29. I. C. McMichael and J.-C. Diels, "Degenerate Four Wave Mixing of Femtosecond Pulses in the Saturable Absorber of a Ring Dye Laser," XIIIth Int. in *Proceedings, Thirteenth International Quantum Electronics Conference* (June 1984), paper MDD2.
30. J. D. Jackson, *Classical Electrodynamics* (Wiley, New York, 1962), pp. 212–215.
31. "Optical Glass," Schott Catalog No. 3111.